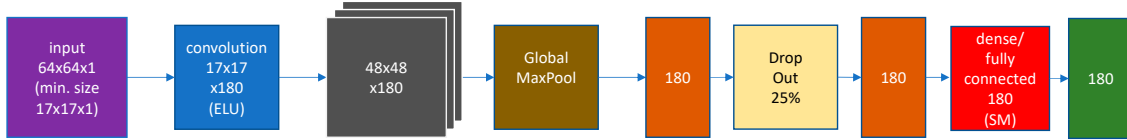
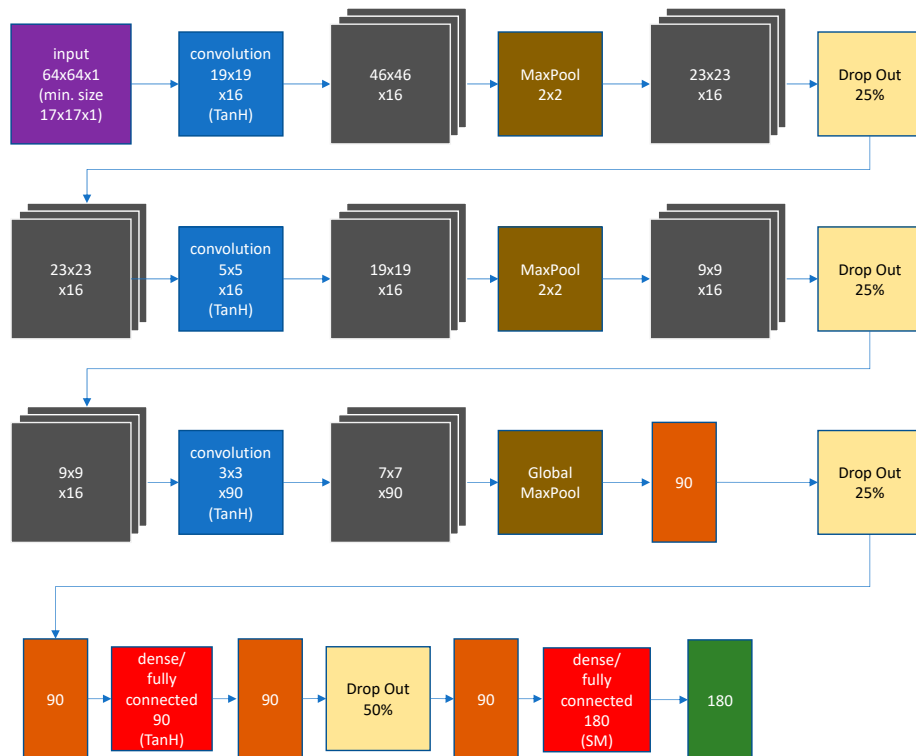


# A Convolutional Neural Networks-Based Approach for Texture Directionality Detection - Supplementary Materials

a) Shallow CNN architecture SN1 with activation function ELU



b) Deep CNN architecture DN1 with activation function TanH



c) Legend

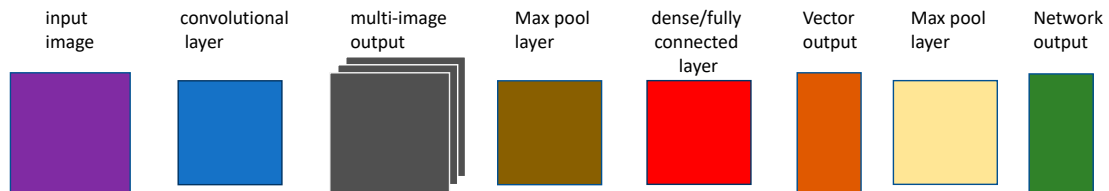


**Figure S1.** Instances of shallow (a) and deep (b) CNN architectures and legend for the diagram blocks (c). In the “convolutional layer” and “dense/fully connected layer” blocks an activation function is reported in parenthesis. The quantities in the “input image” and “multi-image output” blocks will change depending on the size of the input image. The specific quantities shown in the figure represent the size of the images processed in the paper. In the “input image” block the minimum allowed image size is reported in parenthesis.

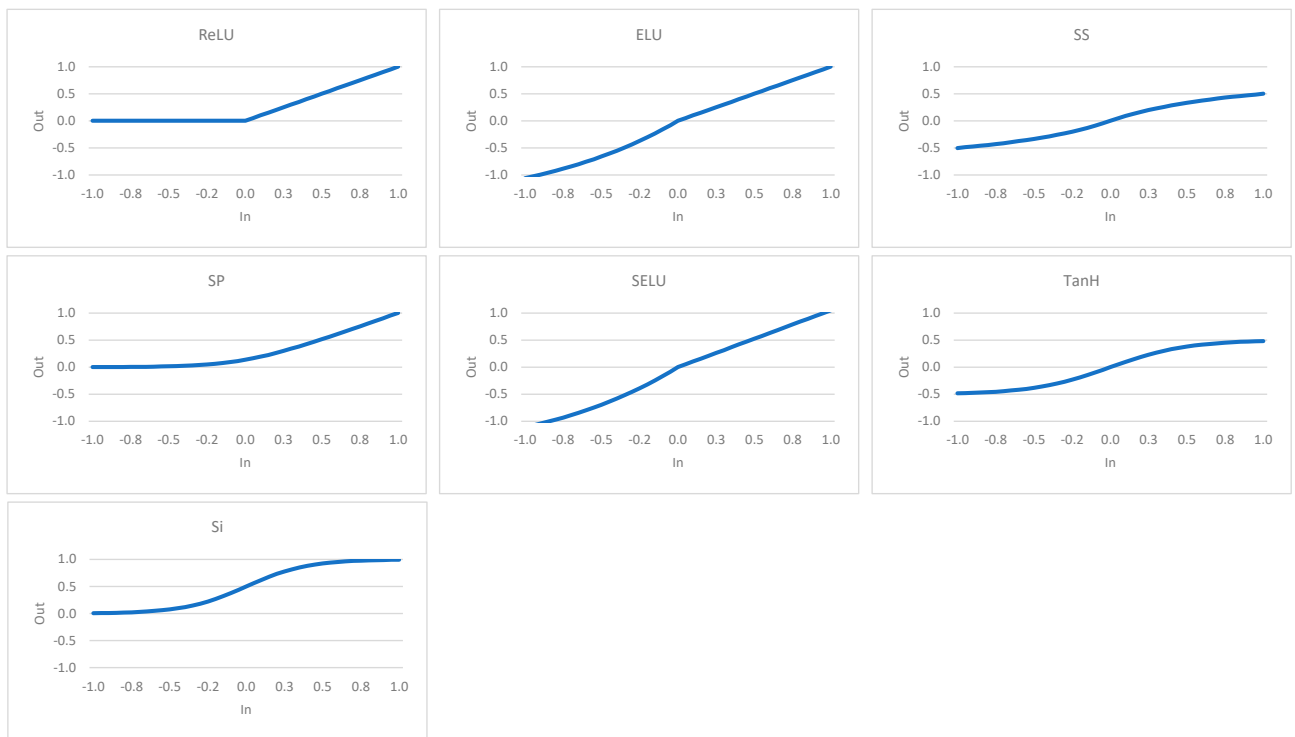


**Figure S2.** Activation functions tested in this work; graphs obtained from equations in [56].

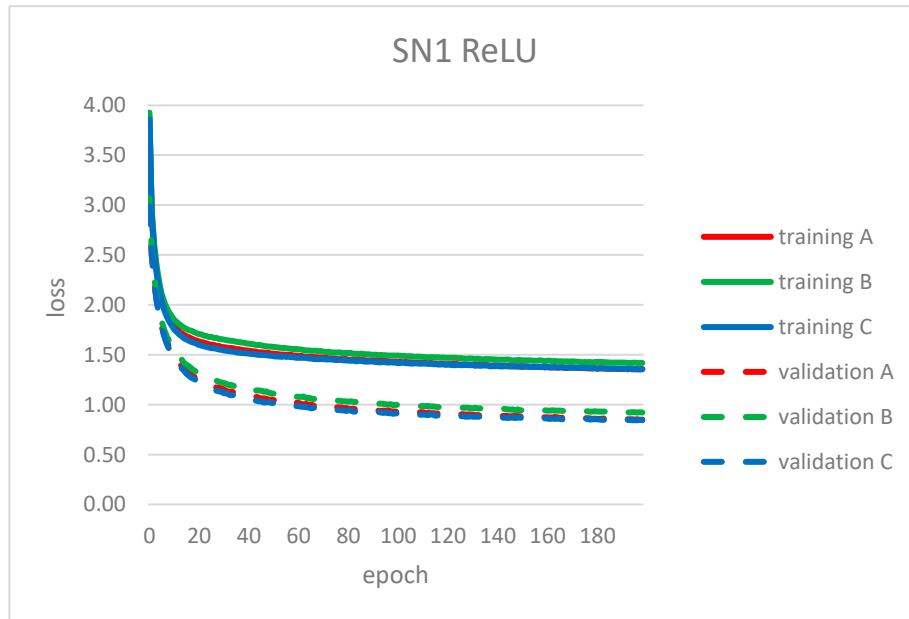


**Figure S3** Training and validation loss curves for the three replicas of SN1 ReLU.

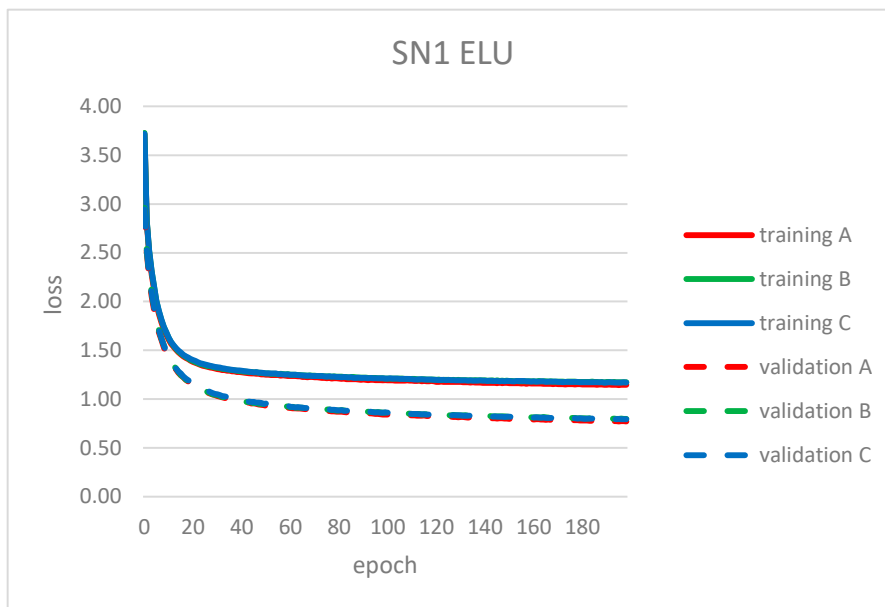


**Figure S4.** Training and validation loss curves for the three replicas of SN1 ELU.

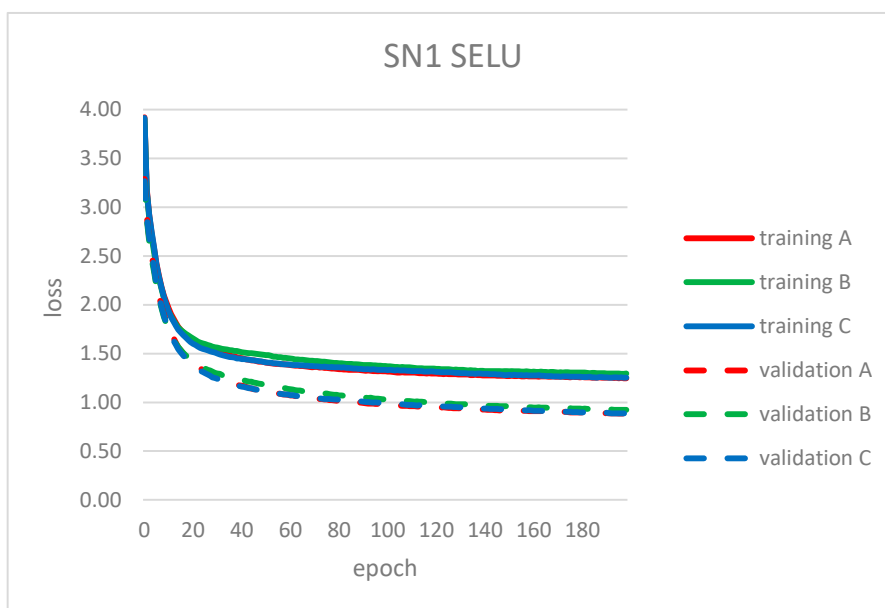


**Figure S5.** Training and validation loss curves for the three replicas of SN1 SELU.

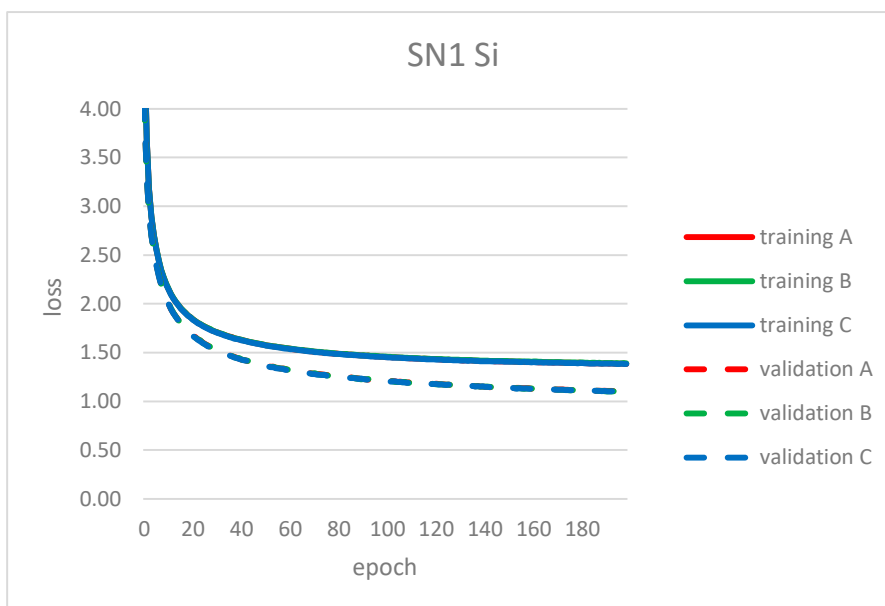


**Figure S6.** Training and validation loss curves for the three replicas of SN1 Si.

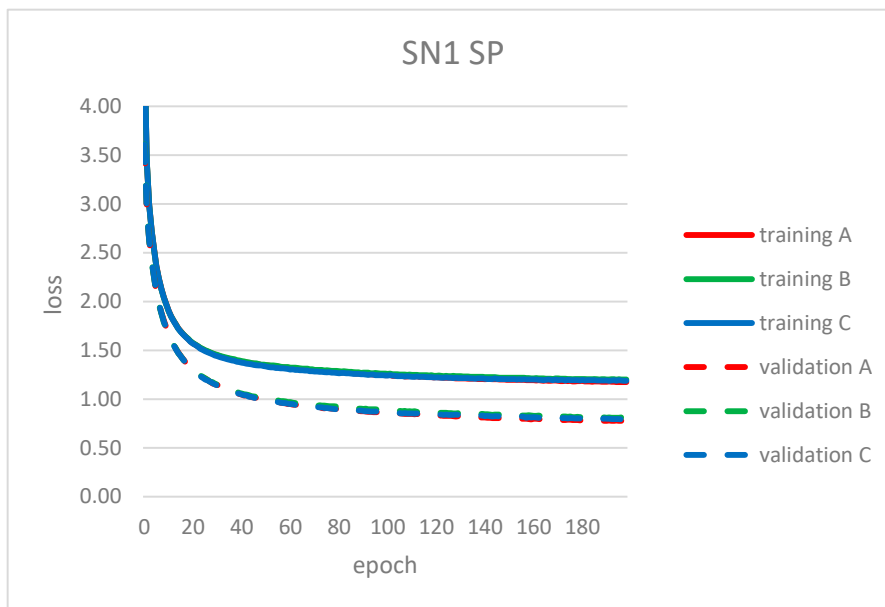


**Figure S7.** Training and validation loss curves for the three replicas of SN1 SP.

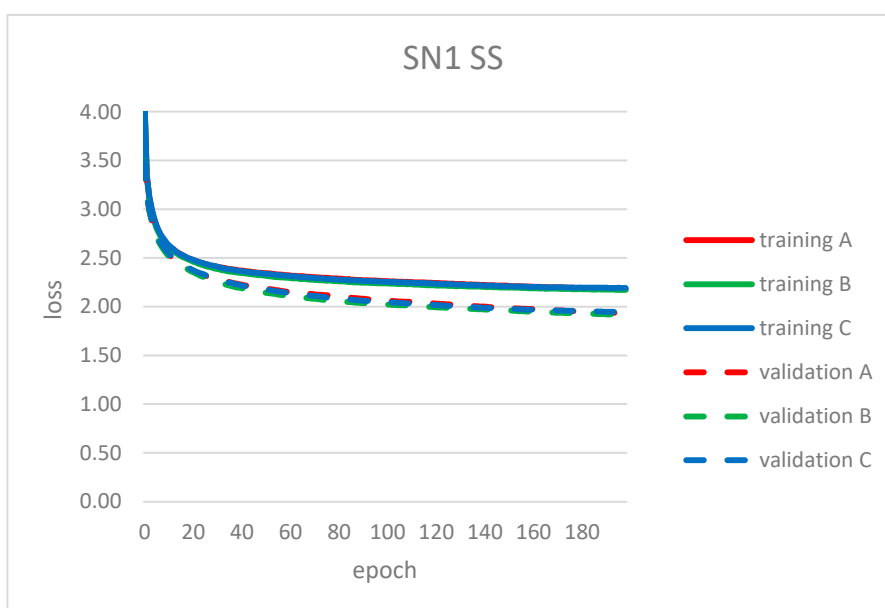


**Figure S8.** Training and validation loss curves for the three replicas of SN1 SS.

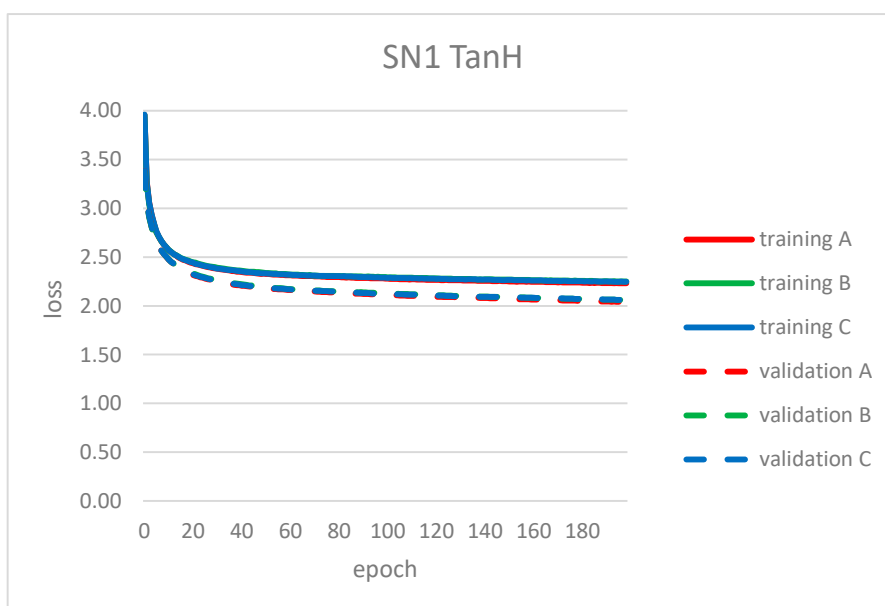


**Figure S9.** Training and validation loss curves for the three replicas of TanH.



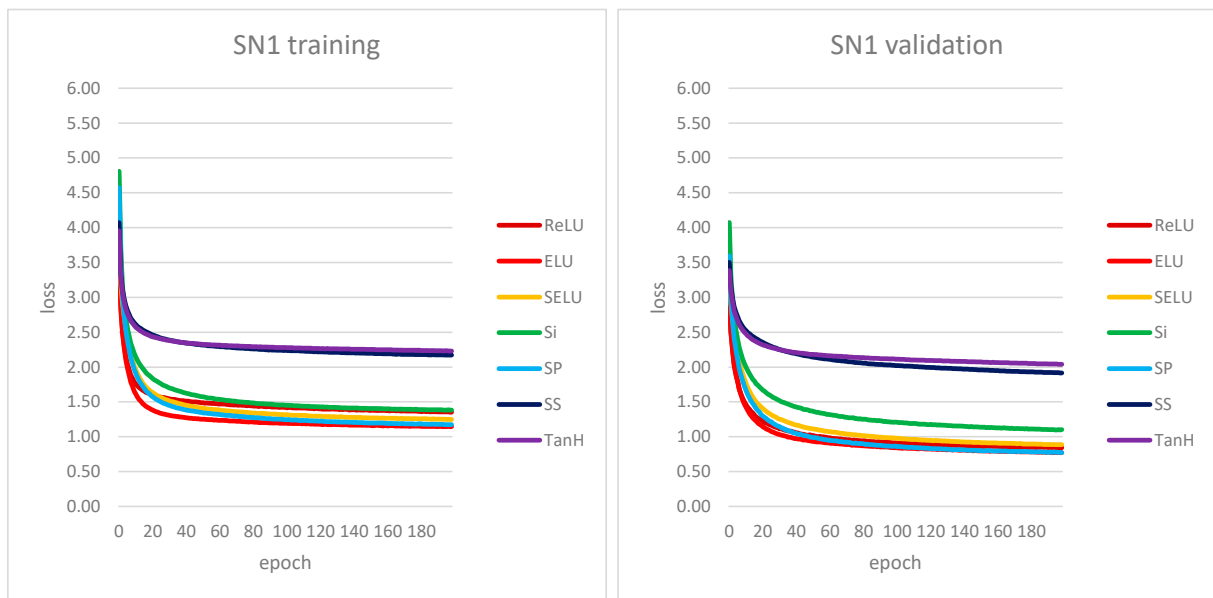


**Figure S10.** Training and validation loss curves for the SN1.

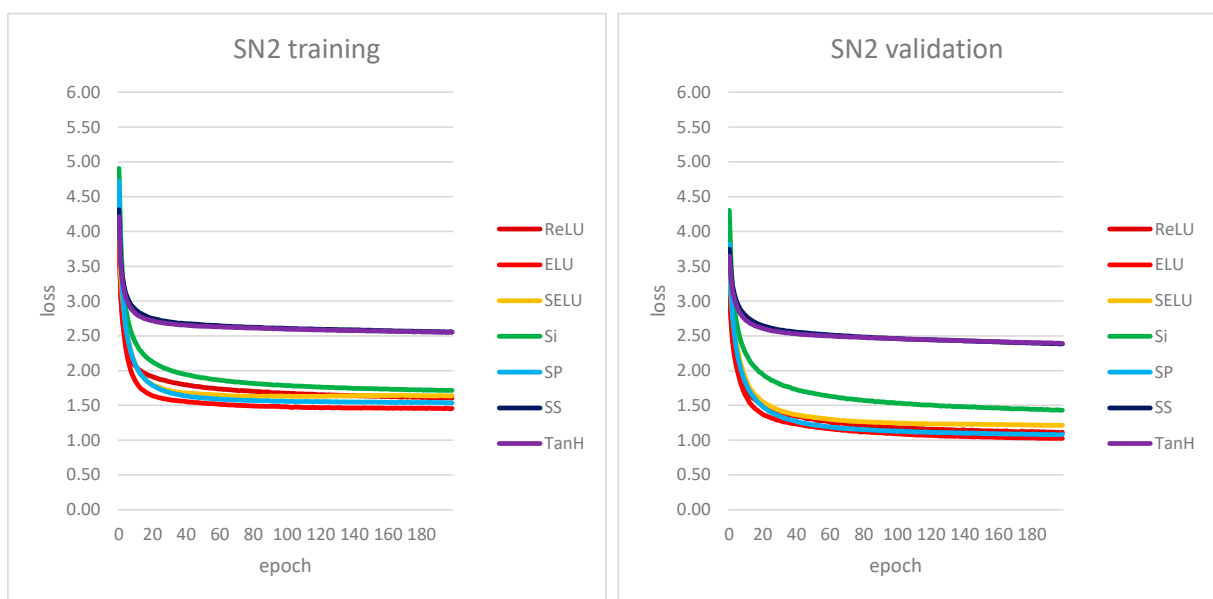


**Figure S11.** Training and validation loss curves for the SN2.

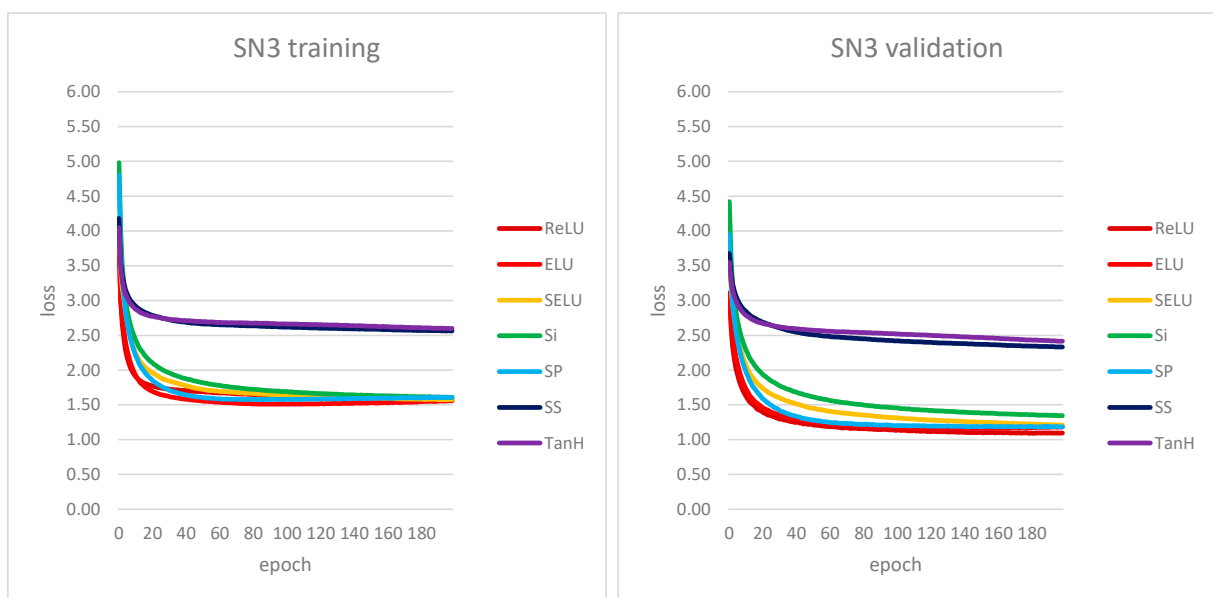


**Figure S12.** Training and validation loss curves for the SN3.

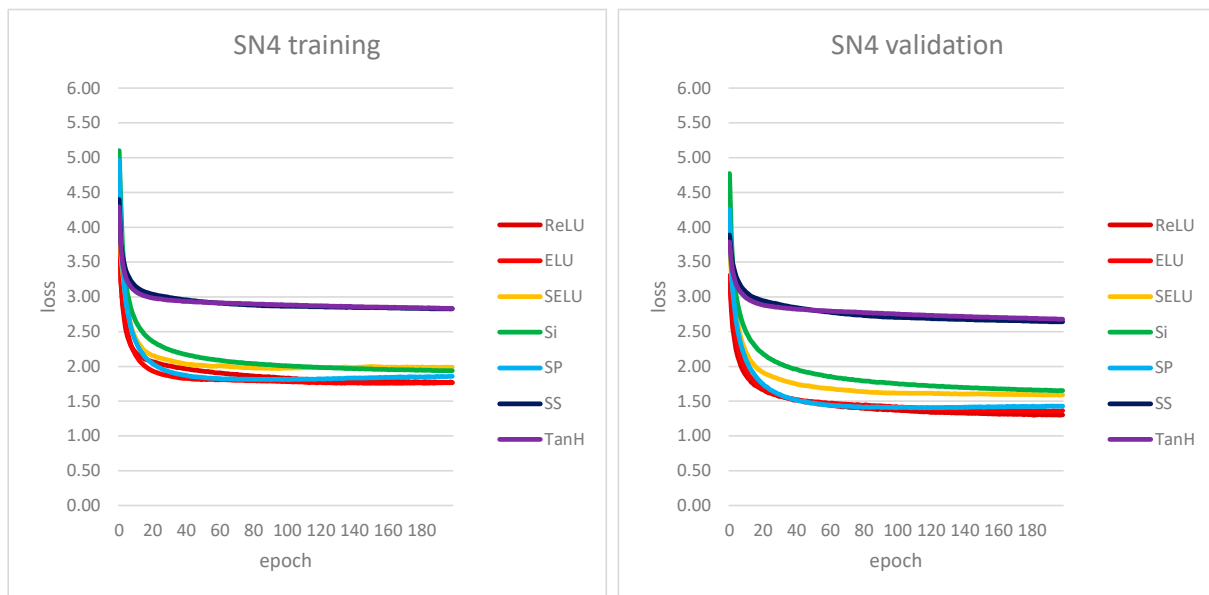


**Figure S13.** Training and validation loss curves for the SN4.

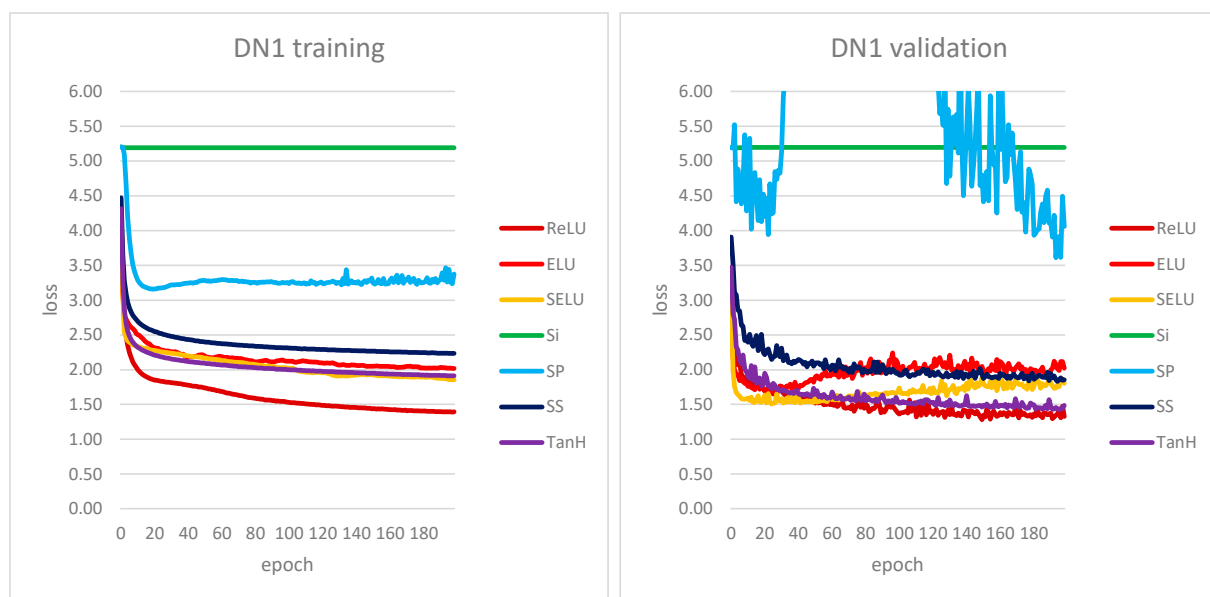


**Figure S14.** Training and validation loss curves for the DN1.

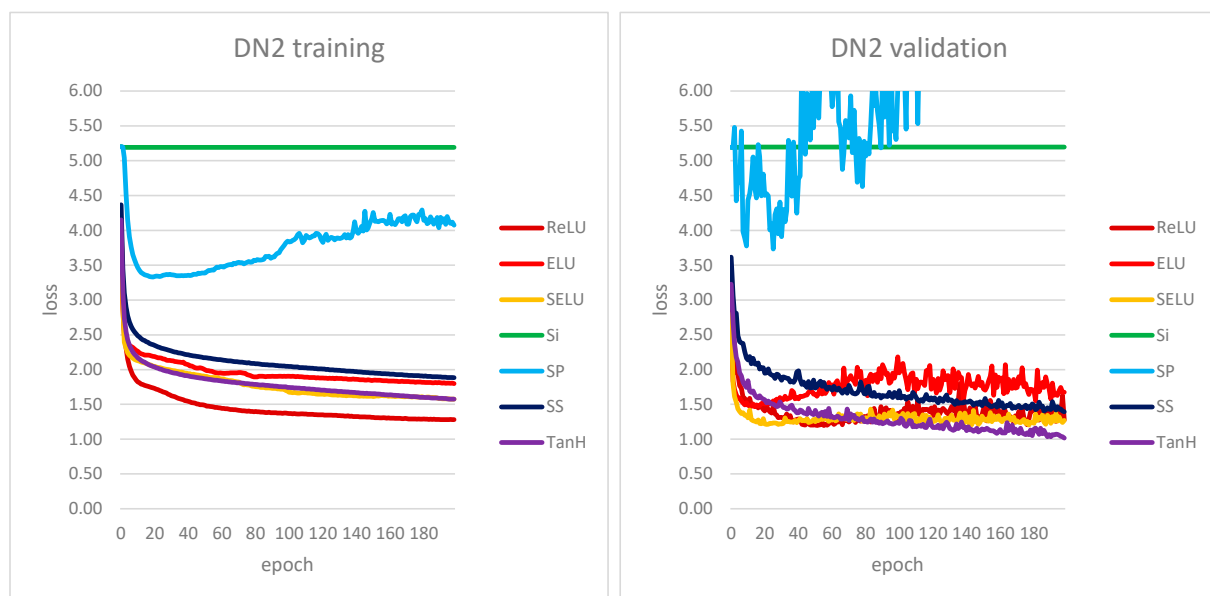


**Figure S15.** Training and validation loss curves for the DN2.

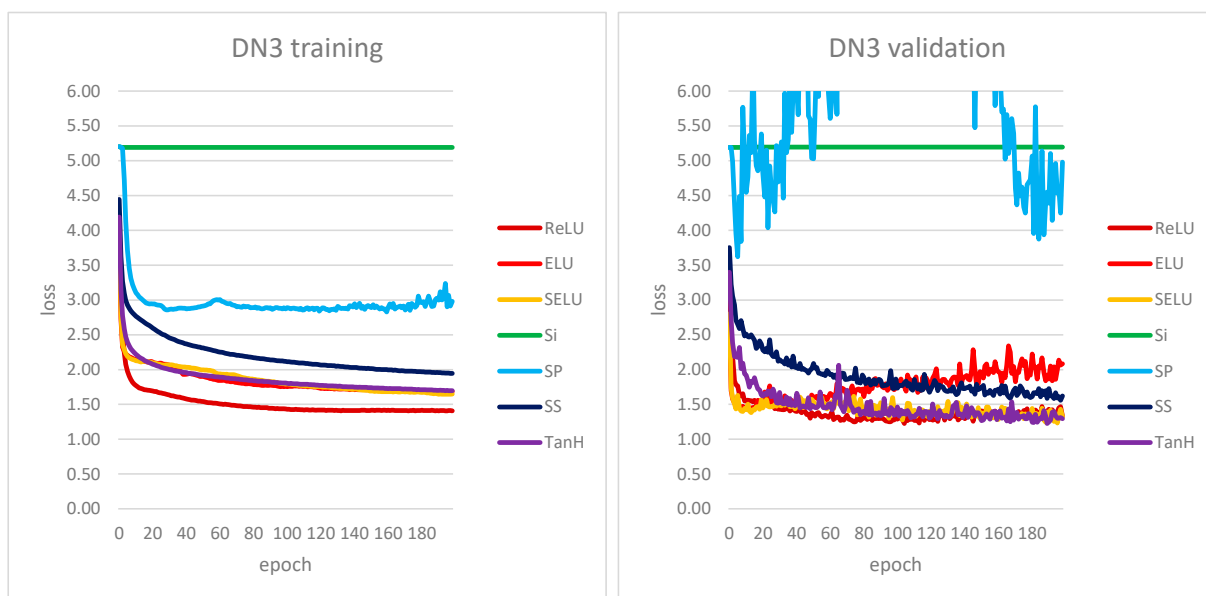


**Figure S16.** Training and validation loss curves for the DN3.

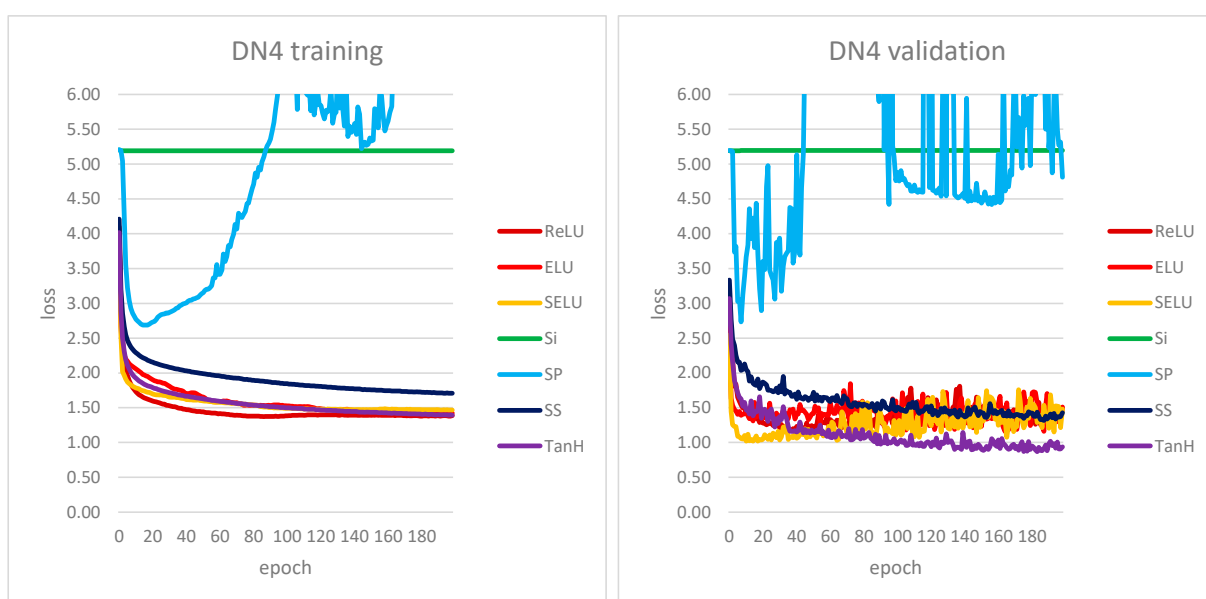


**Figure S17.** Training and validation loss curves for the DN4.

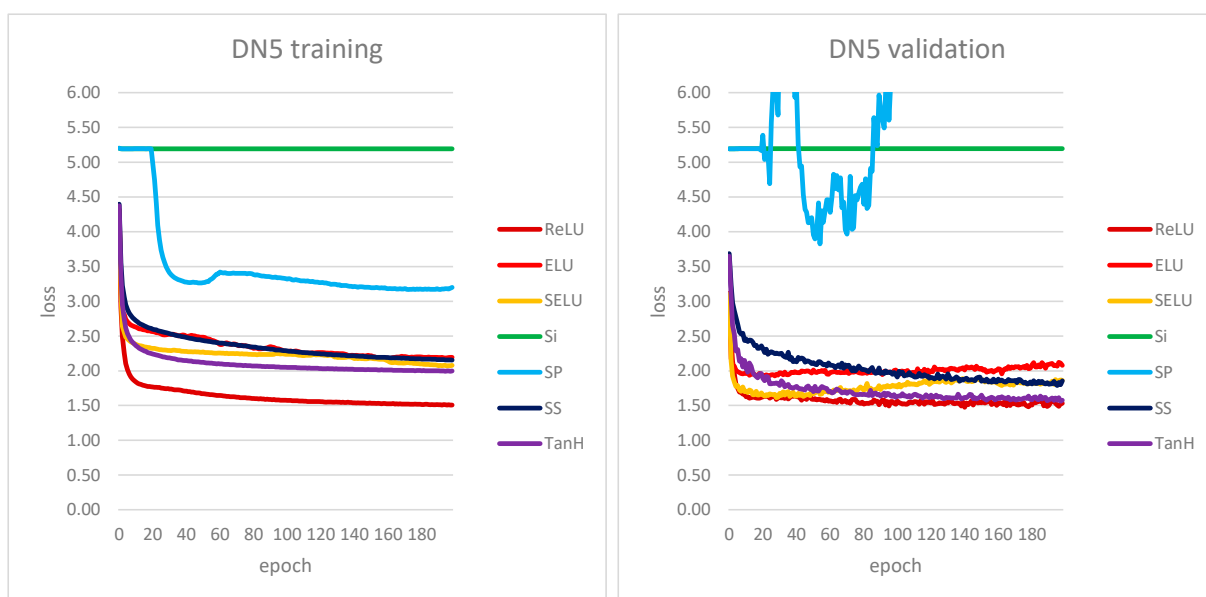


**Figure S18.** Training and validation loss curves for the DN5.

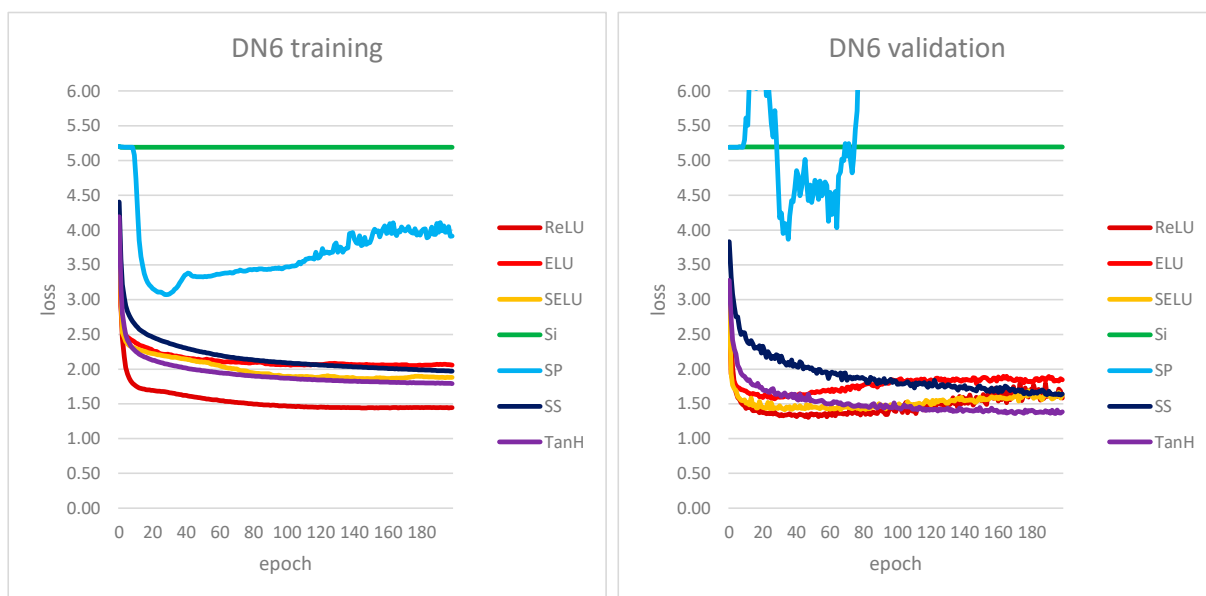


**Figure S19.** Training and validation loss curves for the DN6.

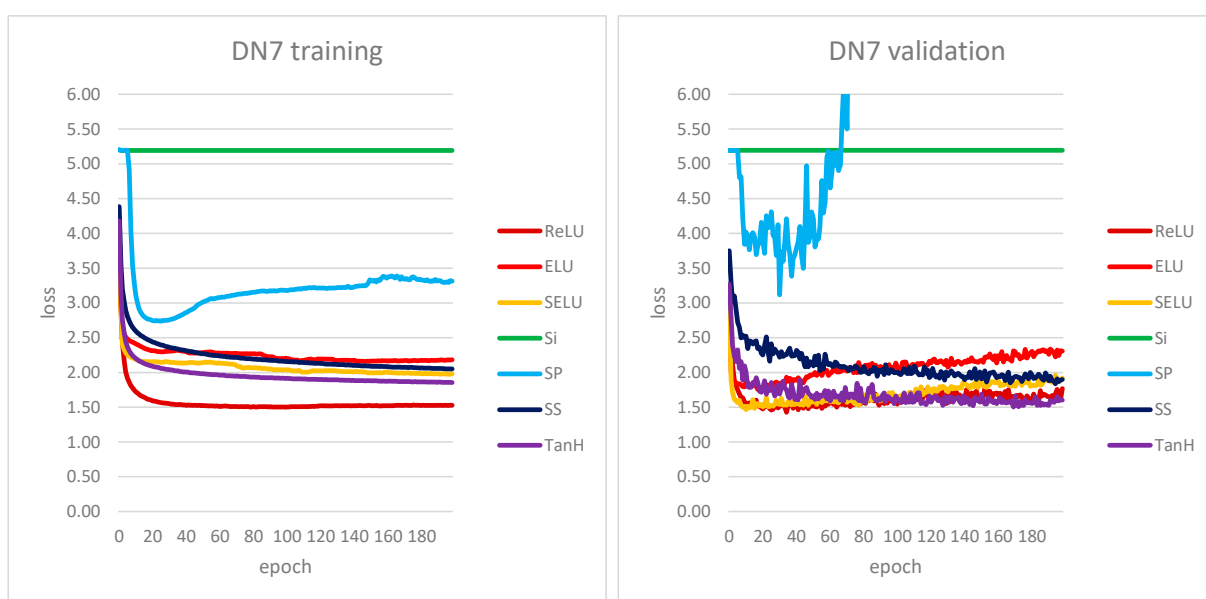


**Figure S20.** Training and validation loss curves for the DN7.

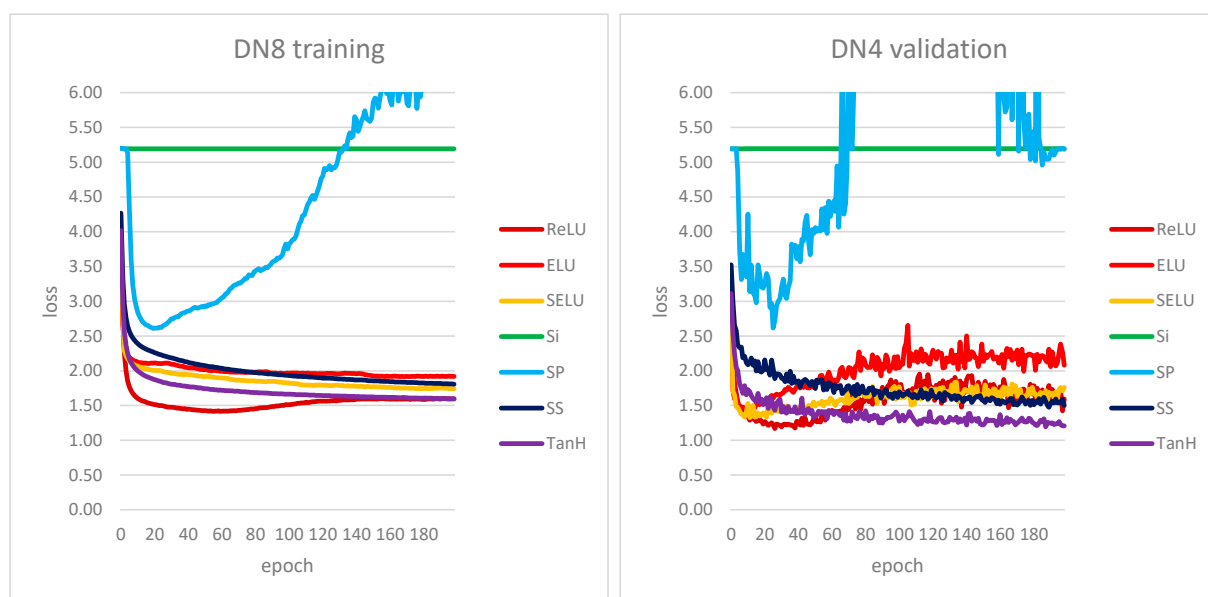


**Figure S21.** Training and validation loss curves for the DN8.

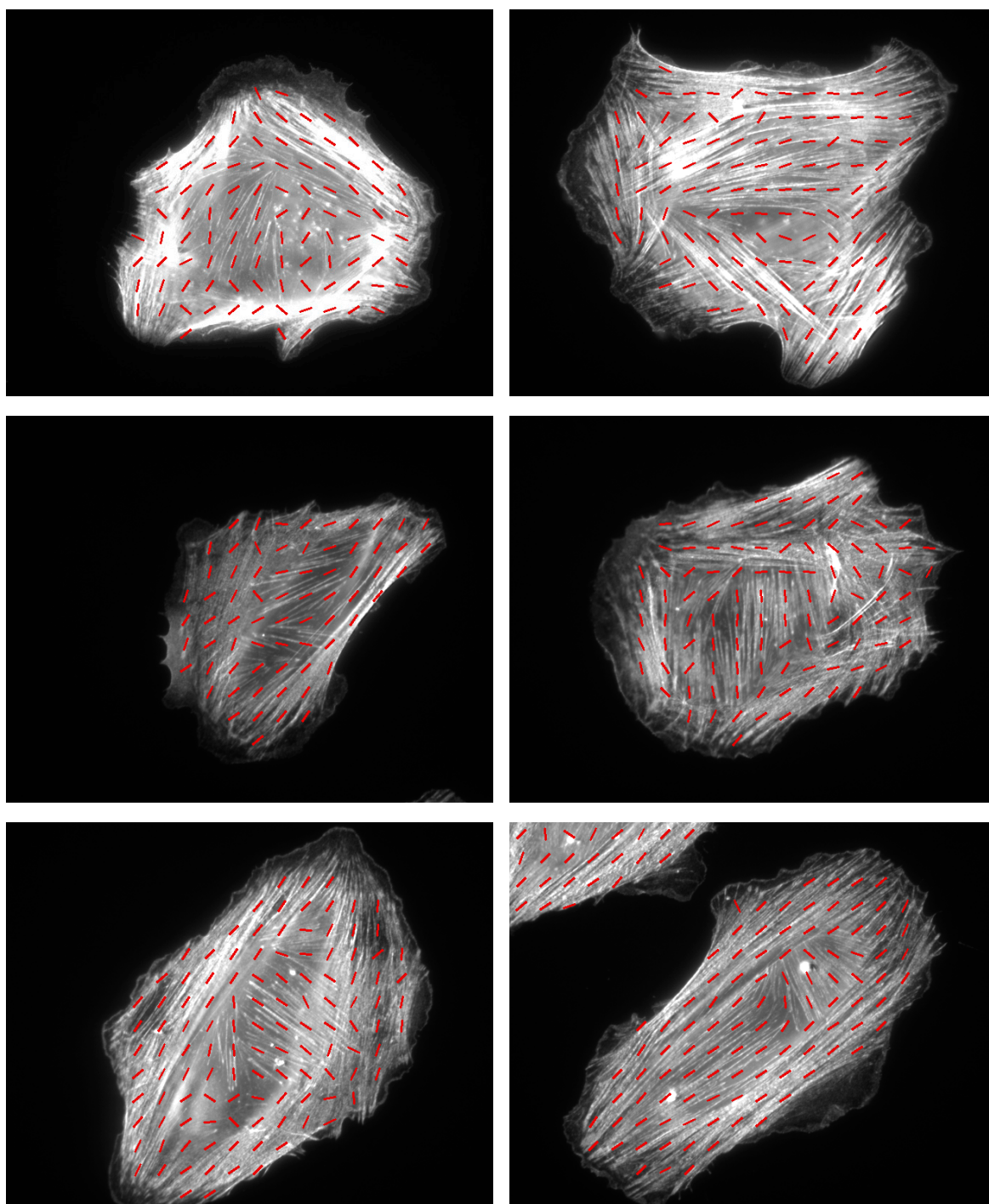


**Figure S22.** CNN-based directionality detection on microcopy images of actin-stained fibroblast cells.

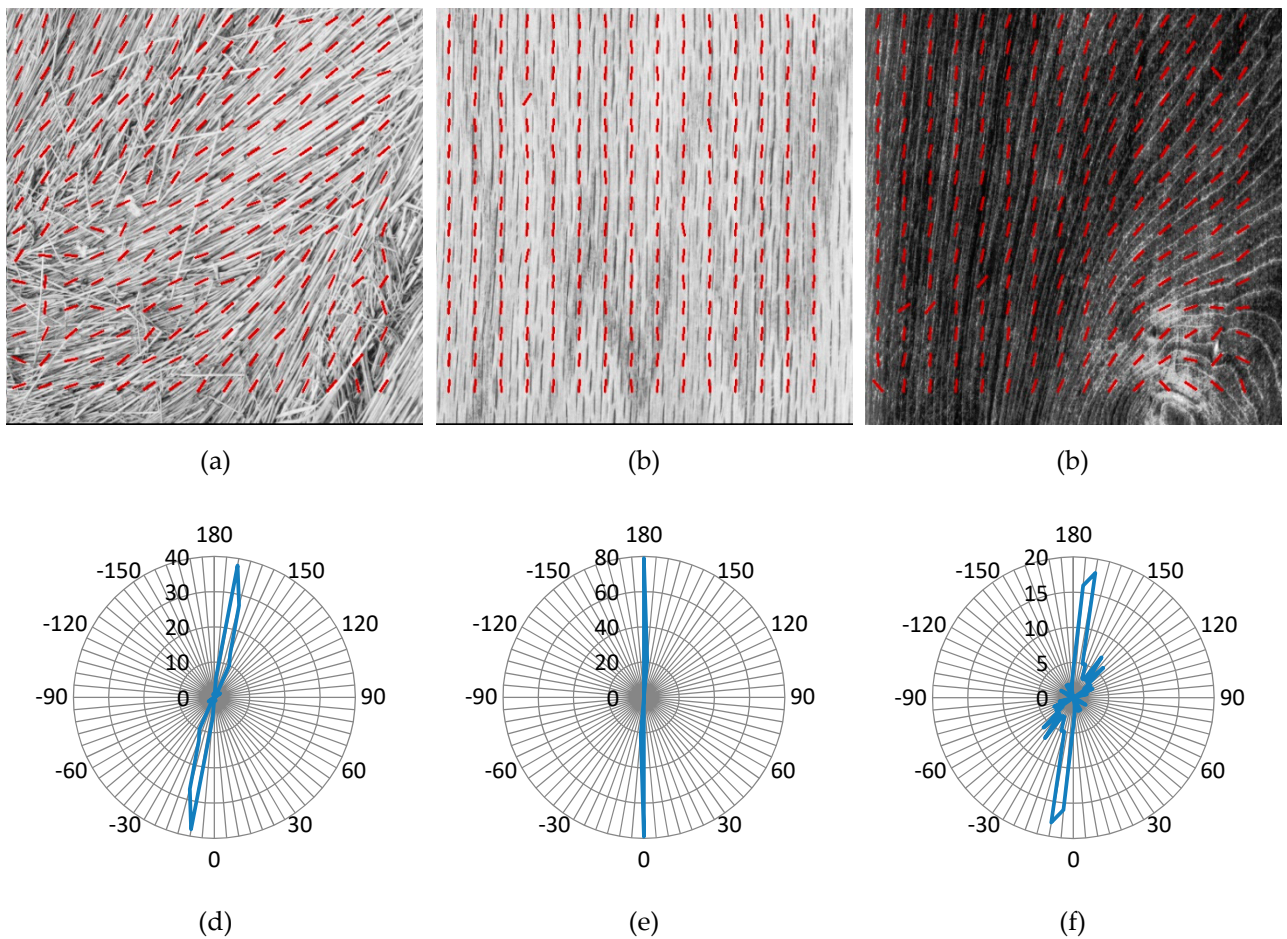


**Figure S23.** CNN-based directionality detection on: (a), (b), (c) Brodatz textures [52,59,60] and corresponding polar plots (d), (e), (f) representing the direction distribution in the analyzed textures.

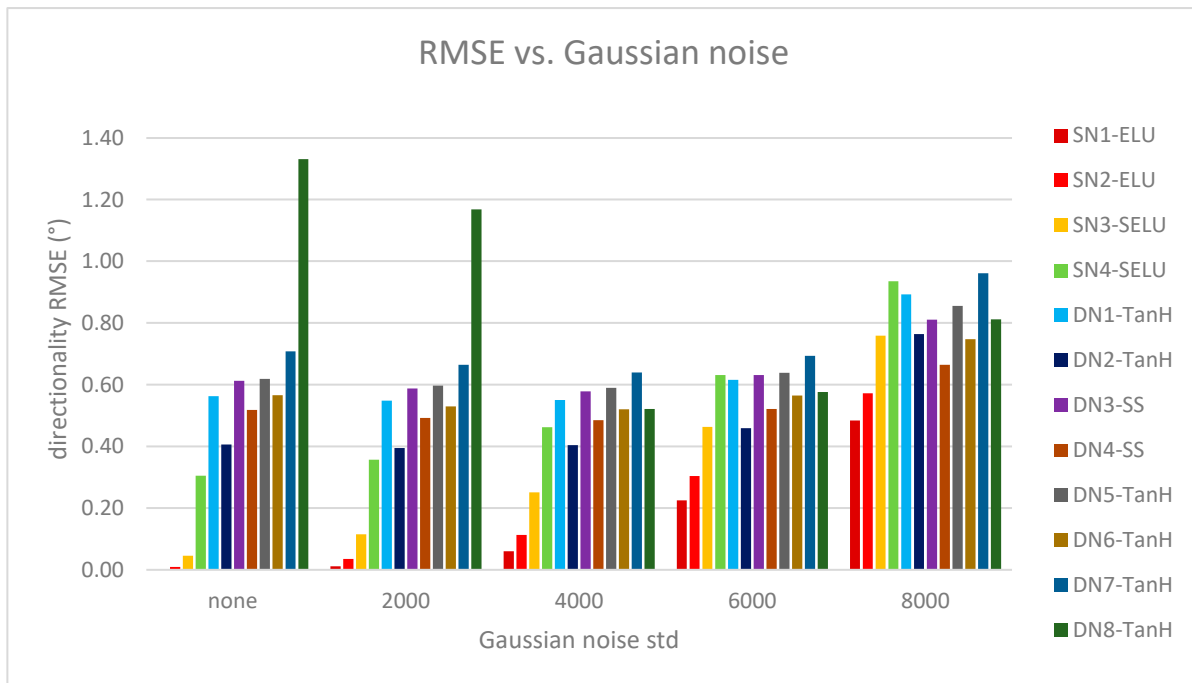


**Figure S24.** Directionality RMSE vs. Gaussian noise standard deviation for all shallow and deep CNNs. The RMSE for each CNN is computed with the respective best performing activation function.



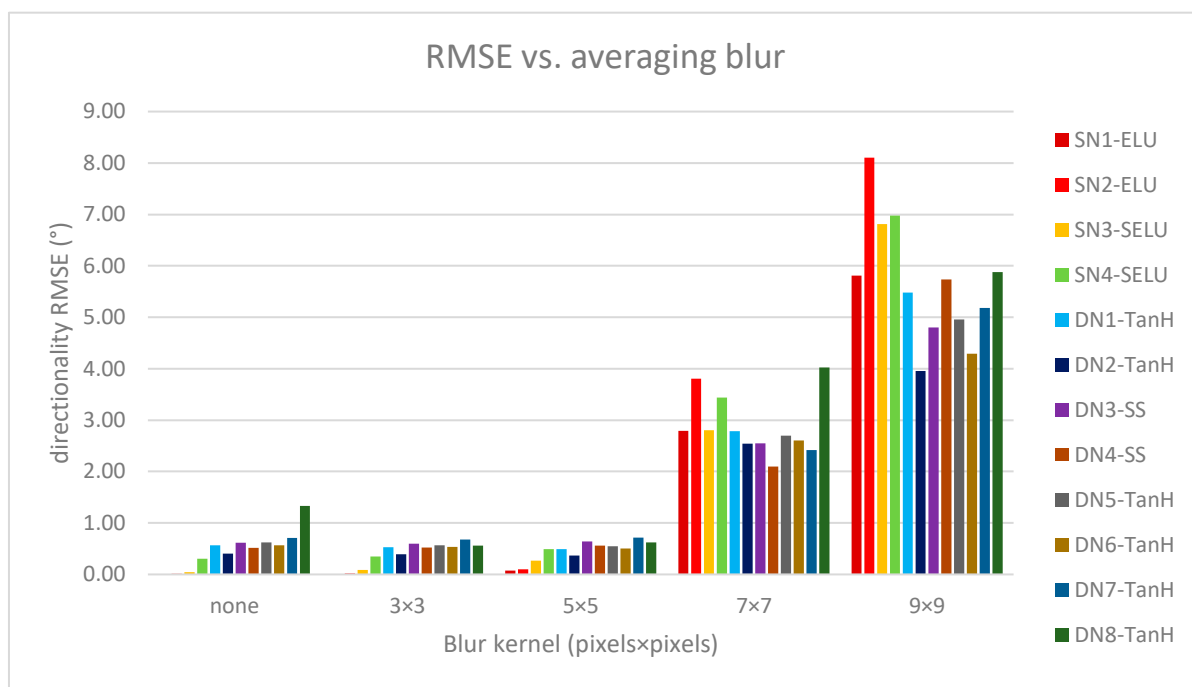
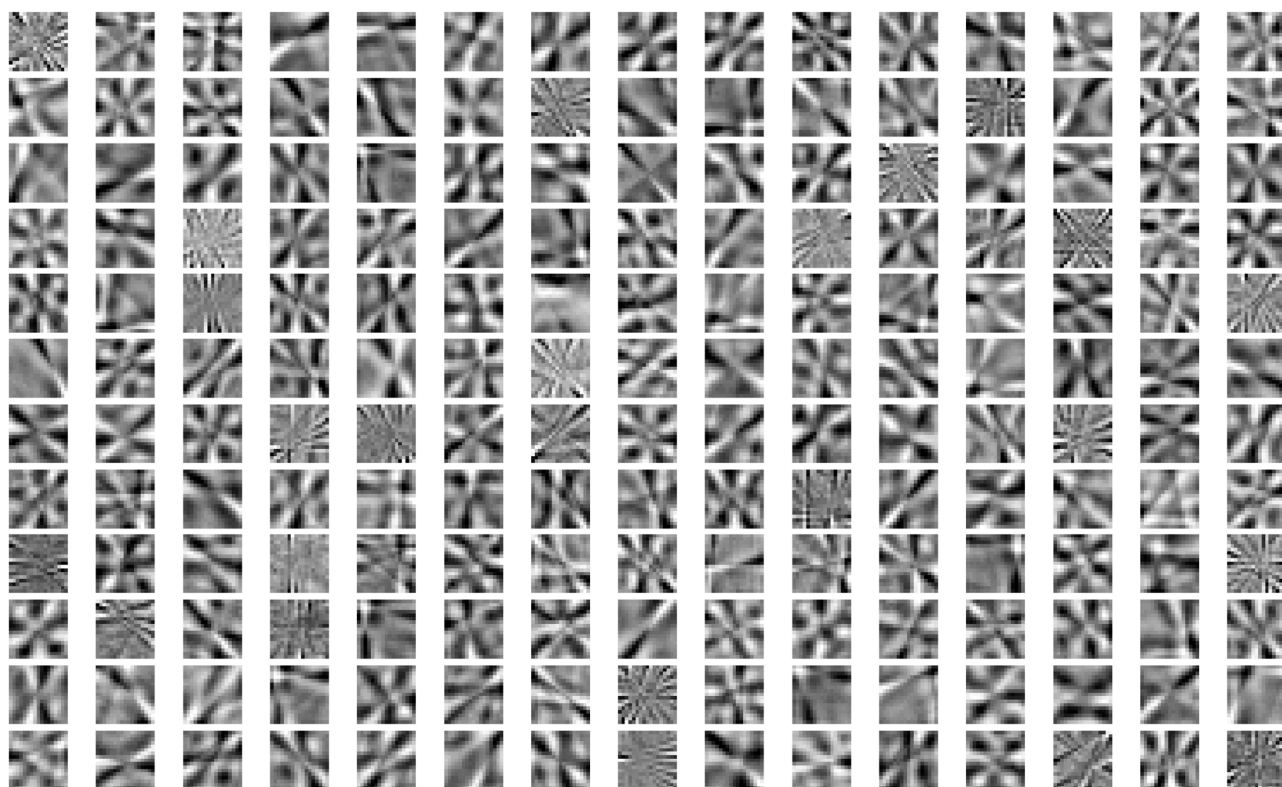
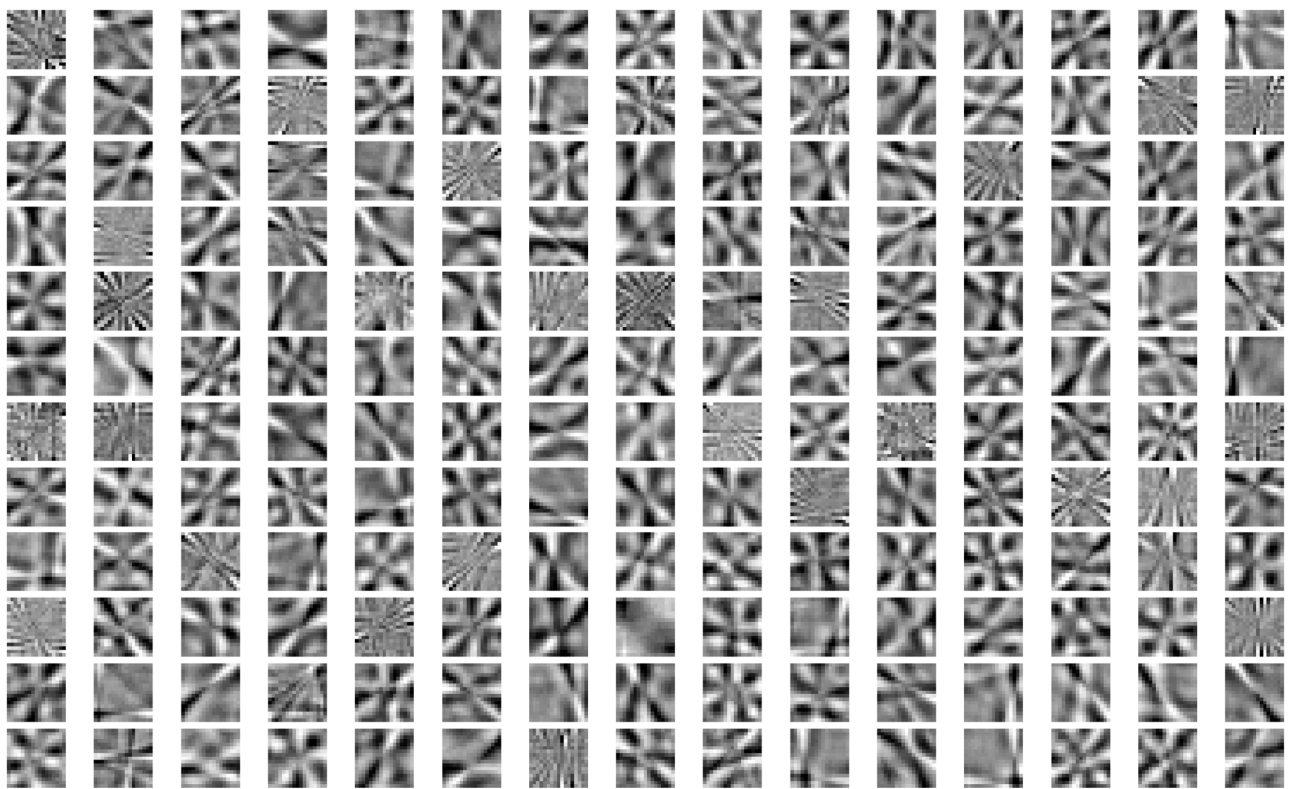


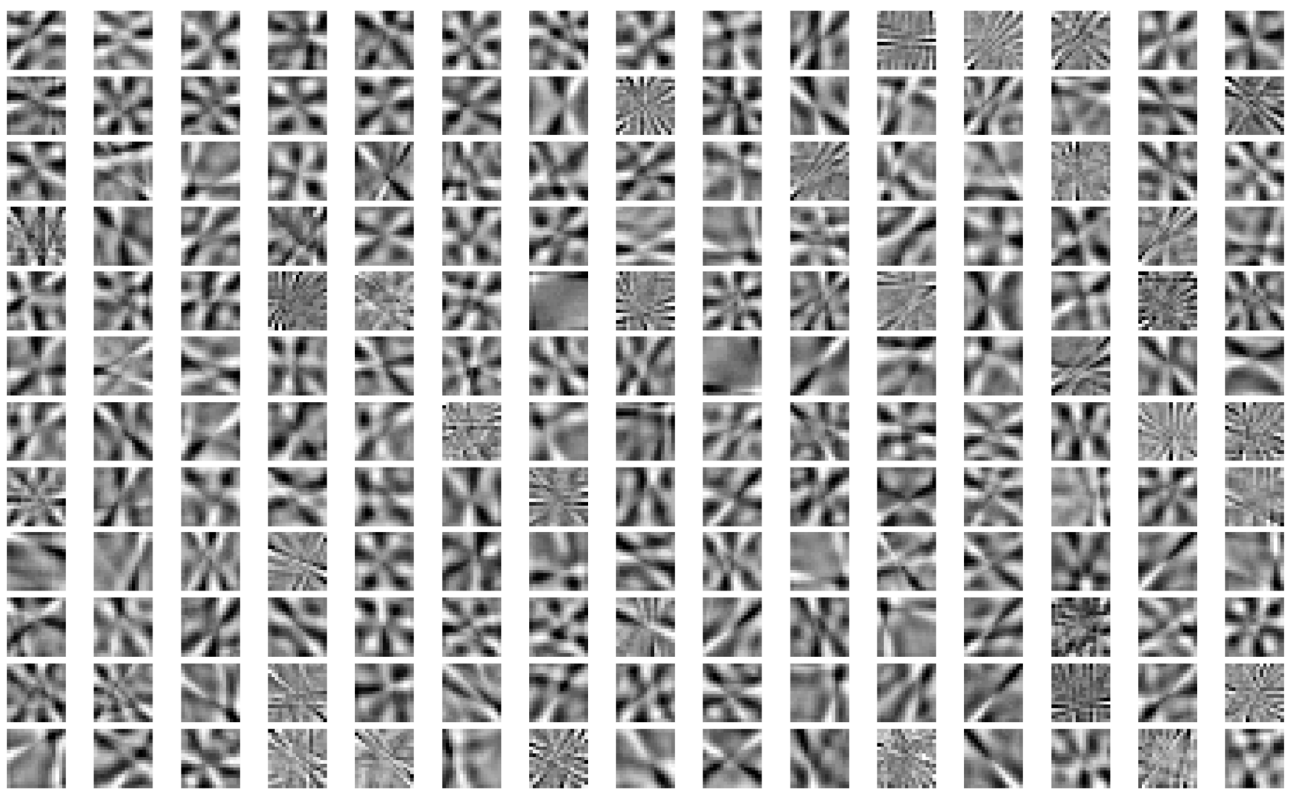
**Figure S25.** Directionality RMSE vs. blur kernel size for all shallow and deep CNNs. The RMSE for each CNN is computed with the respective best performing activation function.



(a)



(b)



(c)

**Figure S26.** Filters from the only convolutional layer of the best shallow CNN, SN1-ELU, for the three training instances (a, b, c, 180 filters each).

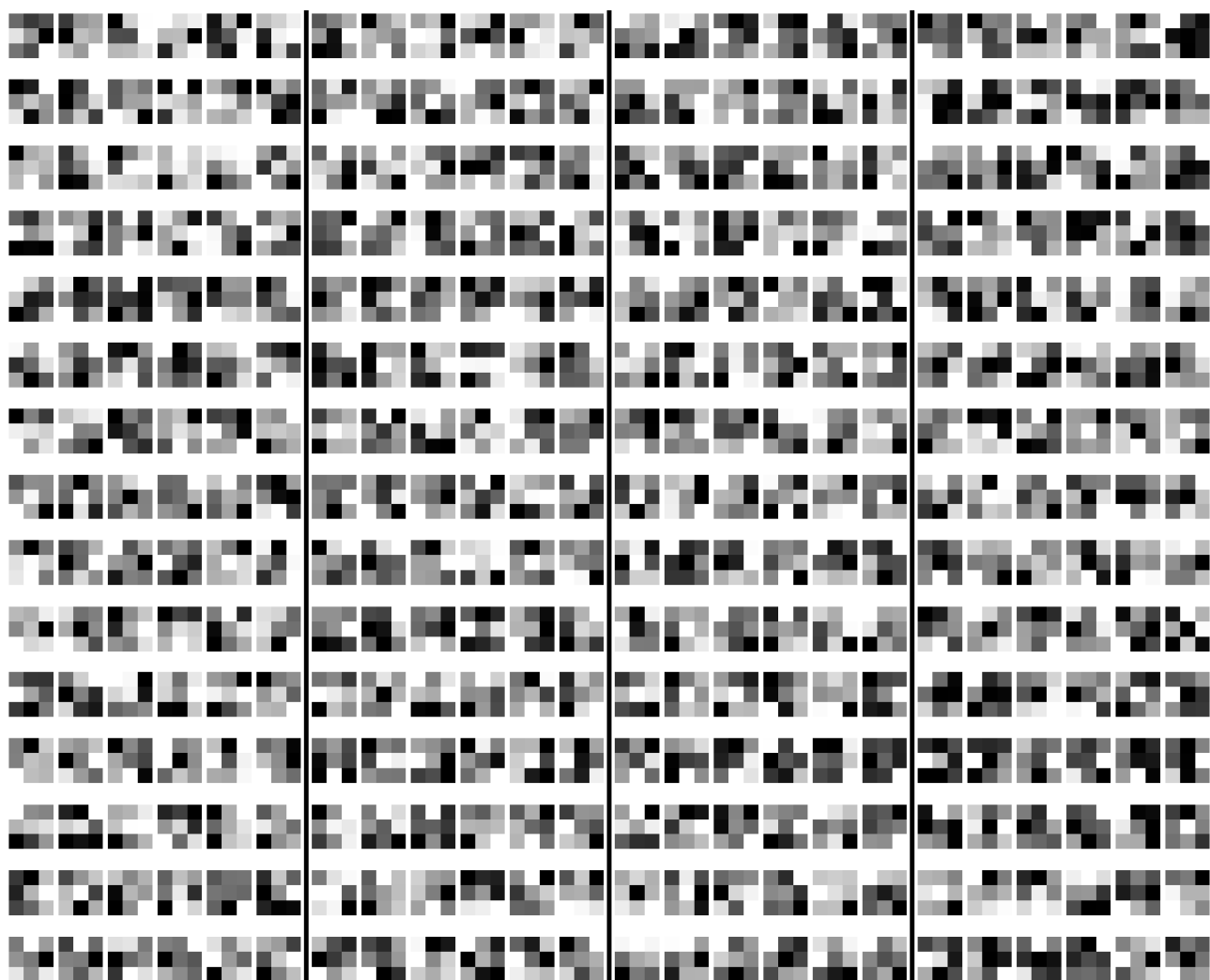




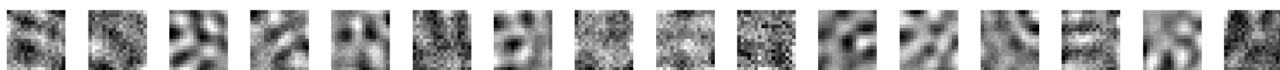
(a) DN2-TanH, first training replicate, first convolutional layer



(b) DN2-TanH, first training replicate, second convolutional layer



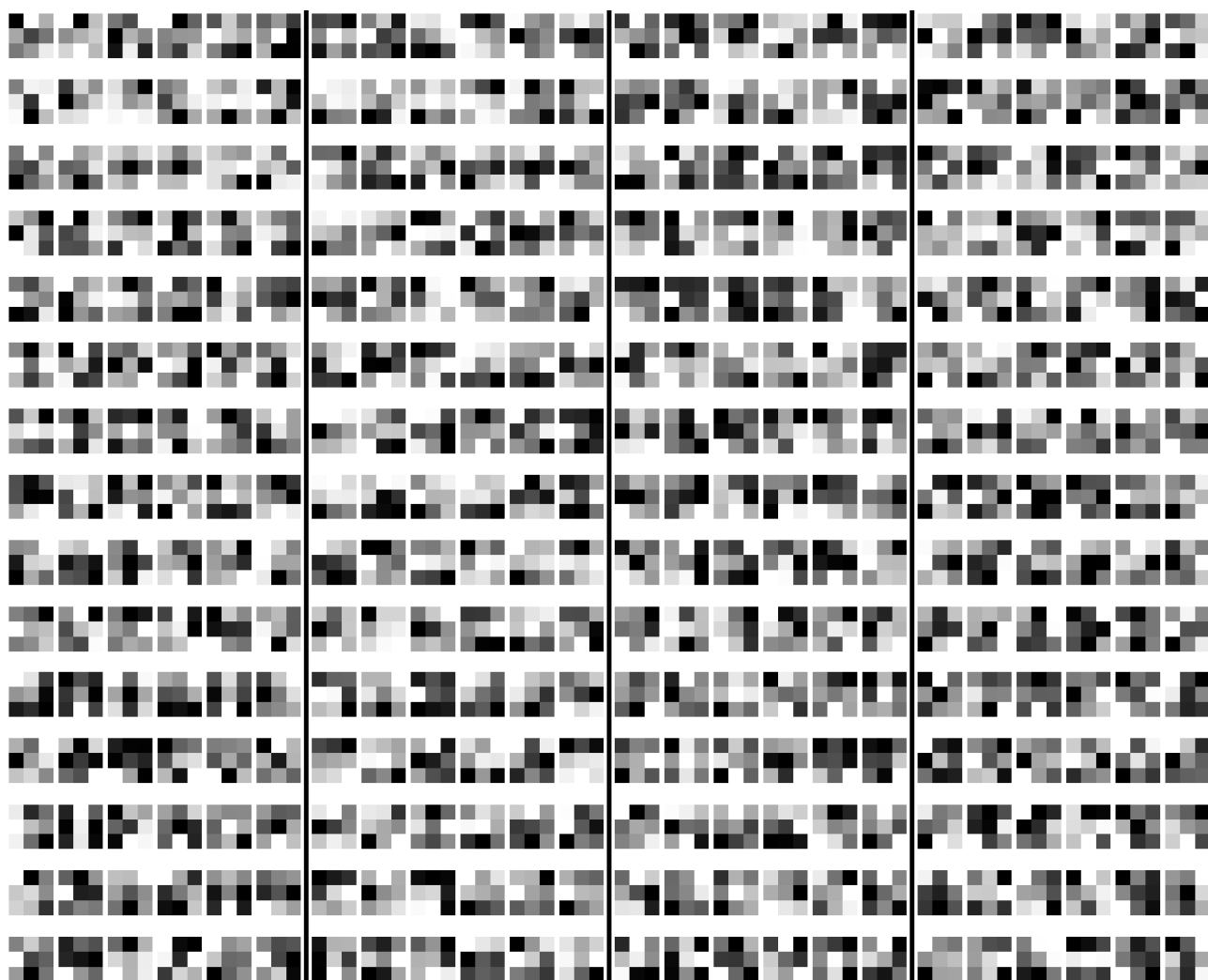
(c) DN2-TanH, first training replicate, third convolutional layer, 4 filter groups out of 32 shown



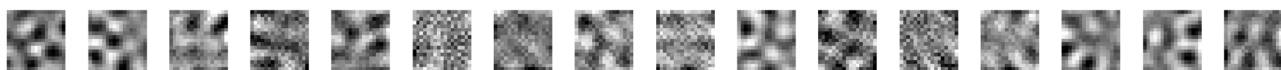
(d) DN2-TanH, second training replicate, first convolutional layer



(e) DN2-TanH, second training replicate, second convolutional layer



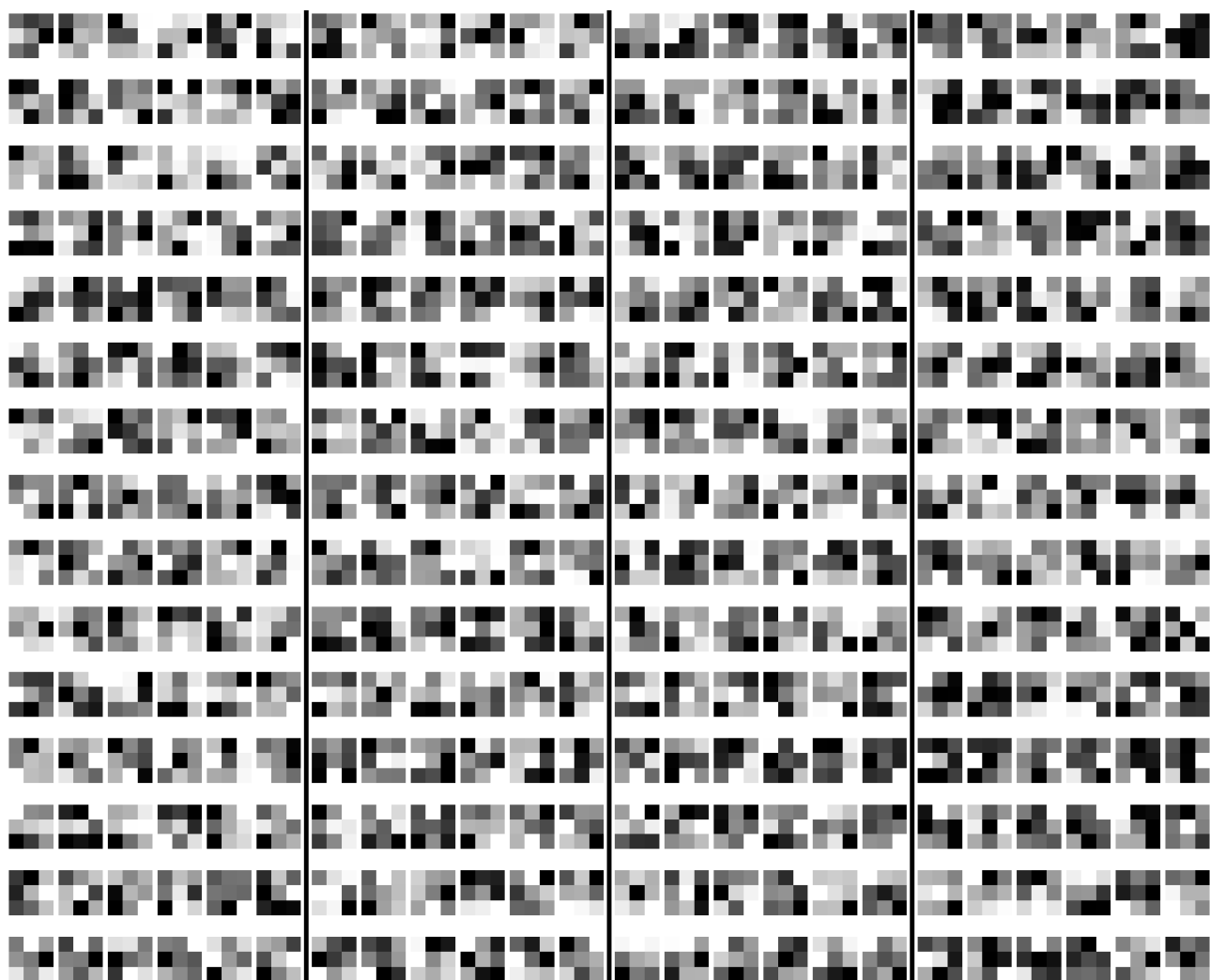
(f) DN2-TanH, second training replicate, third convolutional layer, 4 filter groups out of 32 shown



(g) DN2-TanH, third training replicate, first convolutional layer

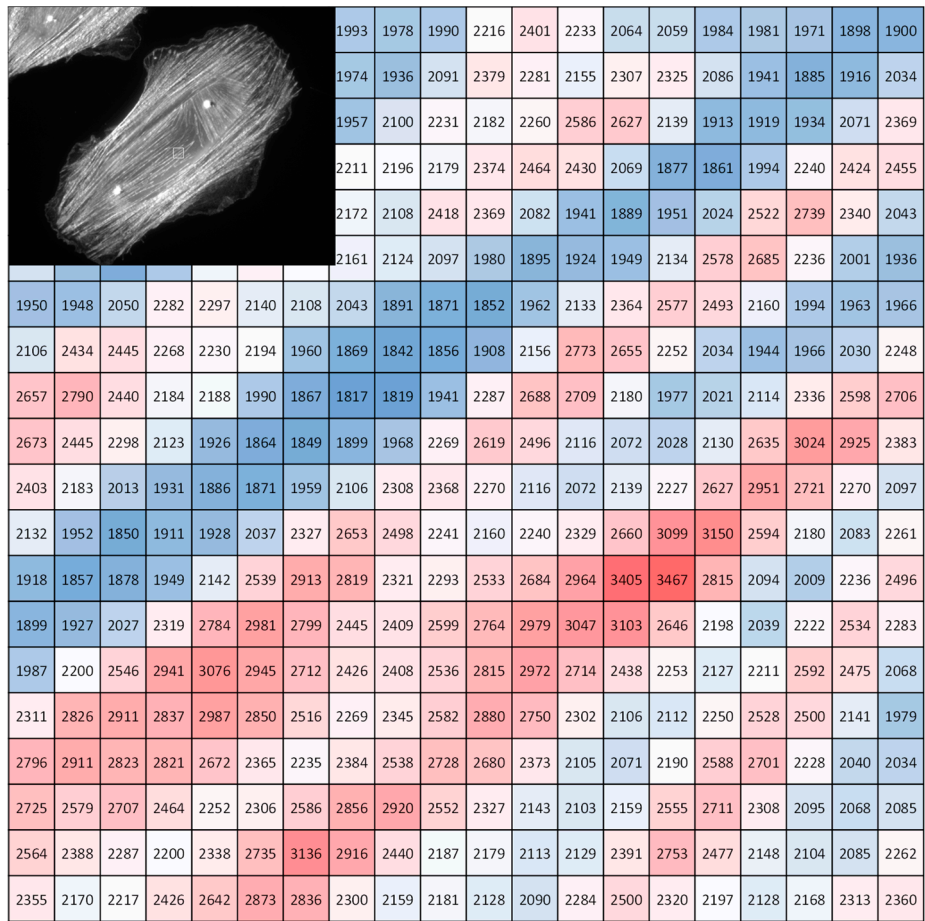


(h) DN2-TanH, third training replicate, second convolutional layer



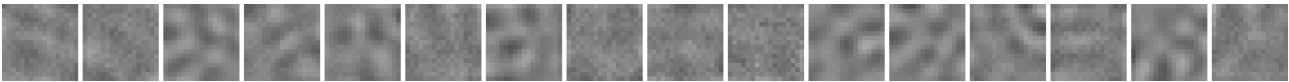
(i) DN2-TanH, third training replicate, third convolutional layer, 4 filter groups out of 32 shown  
*Figure S27. Filters from the convolutional layers of the best deep CNN, DN2-TanH, for the three training replicates.*





(c) actin fibers in fibroblast cell

**Figure S28.** Instances of (a) and (b) synthetic textures and (c) real-life textures with complex signal. The insets show the whole images.



(a)

input texture	1 <sup>st</sup> layer output	intensity std	intensity range
		0.68	1.99
		0.62	1.94
		0.45	1.84
		0.21	1.24
		0.54	2.0
		0.30	1.8

(b)

**Figure S29** Instances of convolutions of synthetic textures with kernels from the first layer of the deep network DN2. The figure shows: (a) 16 17x17 kernels; (b) from left to right: 6 synthetic textures with varying perturbation levels, for each synthetic texture the 16 outcomes of convolution followed by the TanH activation function using the kernels from (a), and the corresponding standard deviation and intensity range values.





(a)

input texture	1 <sup>st</sup> layer output	intensity std	intensity range
		0.47	1.89
		0.36	1.67
		0.25	1.22
		0.14	0,88
		0.46	1.90
		0.20	1.65

(b)

**Figure S30.** Instances of convolutions of synthetic textures with kernels from the first layer of the deep network DN6. The figure shows: (a) 16 7x7 kernels; (b) from left to right: 6 synthetic textures with varying perturbation levels, for each synthetic texture the 16 outcomes of convolution followed by the TanH activation function using the kernels from (a), and the corresponding standard deviation and intensity range values.

**Table S1.** Performance comparison between the best shallow and deep CNNs.

	SN1-ELU	DN2-TanH
Gaussian noise std value	RMSE (°)	RMSE (°)
none	0.00	0.41
2000	0.01	0.39
4000	0.06	0.40
6000	0.23	0.46
8000	0.48	0.76

	SN1-ELU	DN2-TanH
Blur kernel size	RMSE (°)	RMSE (°)
none	0.00	0.41
3x3	0.01	0.39
5x5	0.07	0.37
7x7	2.79	2.54
9x9	5.81	3.39

	SN1-ELU	DN3-TanH
# tiles tested	(tiles/s)	(tiles/s)
178 605	6613.3	6821

**Table S2.** Directionality RMSE values vs. Gaussian noise standard deviation and averaging blur for deep networks DN2-TanH (first filter kernel 17x17) and DN6-TanH (first filter kernel 7x7)..

	DN2-TanH	DN12-TanH
Gaussian noise std value	RMSE (°)	RMSE (°)
none	0.41	0.57
2000	0.39	0.53
4000	0.40	0.52
6000	0.46	0.57
8000	0.76	0.75

	DN2-TanH	DN12-TanH
Blur kernel size	RMSE (°)	RMSE (°)
none	0.41	0.57
3x3	0.39	0.53
5x5	0.37	0.51
7x7	2.54	2.61
9x9	3.39	4.29